Surface-grafted metal oxide clusters and metal carbonyl clusters in zeolite micropores; XAFS/FTIR/TPD characterization and catalytic behavior

Masaru Ichikawa [a,*], Wei Pan [a,1], Yasunori Imada [a], Masatugu Yamaguchi [a], Kiyoshi Isobe [b], Takafumi Shido [a]

[a] *Catalysis Research Center, Hokkaido University, Sapporo 060, Japan*
[b] *Department of Chemistry, Faculty of Science, Osaka City University, Izumi, Osaka 586, Japan*

Abstract

SiO_2-grafted $[(\mu_3\text{-}C_4H_7)_2Rh]_2V_4O_{12}$ and $[(RhCp^*)_4V_6O_{19}]$ as molecular models of supported Rh catalysts characterized by EXAFS, FTIR, and TPD exhibit high catalytic activities for selective oxidation of propene towards acetone. SiO_2-impregnated triple cubane-type complete $[(RhCp^*)_4 Mo_4O_{16}]$ and incomplete $(RhCp^*)_2Mo_3O_9(OMe)_4$ were reduced under photoillumination (> 365 nm) in CO at 300 K, forming two sets of the intense carbonyl bands at (2061 and 2021 cm^{-1}) and (2092 and 2035 cm^{-1}). All the carbonyls attracted to Rh and Mo sites were eliminated by the thermal evacuation at 330–440 K, leaving oxygen-deficient sites of Mo in the cubane–oxide clusters, which exhibited high catalytic activities for propene metathesis at 300–343 K. We have conducted the low-temperature homologation of methane on a series of zeolite-entrapped Ru, Rh, Co and Pt catalysts which were prepared from $Ru_3(CO)_{12}/NaY$, $H_4Ru_4(CO)_{12}/NaY$, $[HRu_6(CO)_{18}]^-/NaY$, $Co_4(CO)_{12}/NaY$, $Rh_6(CO)_{16}/NaY$, $[Pt_3(CO)_3(\mu_2\text{-}CO)_3]_n^{2-}$ ($n = 3$, 4)/NaY. The carbon species $[CH_x]$ ($x = 0$–3) are deposited on naked metal clusters in NaY by admission of methane at 423–623 K, which are stoichiometrically converted by hydrogen at 300–423 K towards C_1–C_5 hydrocarbons without any formation of graphic carbons. The yields of C_2^+ hydrocarbons in methane homologation were affected by the size of Ru clusters and carbon coverage θc, as follows; $Ru_3/NaY < Ru_4/NaY < Ru_6/NaY < Ru$ (50 Å) on NaY; The reactivity of surface carbon bound to metal clusters in zeolites and mechanism for C–C bond formation are discussed in conjunction with Ru ensemble-size effects and intrazeolitic chemical circumstances.

1. Introduction

Some metal/alloy cluster compounds such as $[Rh_{6-x}Ir_x(CO)_{16}]$ ($x = 0$–6) and $[Pt_3(CO)_3(\mu_2\text{-}CO)_3]_n^{2-}$ ($n = 3$–5) and metal oxide/sulfide clusters have been of interest as molecular precursors grafted on oxide surfaces and encapsulated in zeolite microporous space, because of the promise of such systems for rational preparation of tailor-made metal catalysts [1] and quantum dots/wires for electronic devices [2]. They consist of nanostructured metal aggregates of uniform sizes and discrete metal compositions [3,4]. The heterometallic $Rh_{6-x}Fe_x$ ($x = 2$, 3) [5,6], $Ir_{4-x}Fe_x$ ($x = 1, 2, 3$) [7] and $Ru_{3-x}Co_x$

(x = 1, 2, 3) [8,9] carbonyl clusters localized at the silica interface are demonstrated to be associated with two-site activation of CO to promote the migratory insertion to M–alkyl and M–H in the olefin hydroformylation [6,8] and CO + H_2 reactions to C_1–C_5 alcohols [10].

Recently, novel organometallic oxide clusters such as $[(MCp^*)_4Mo_4O_{16}]$ and $[(MCp^*)_4V_6O_{19}]$ (M = Rh, Ir; Cp* = pentamethylcyclopentadiene) have been synthesized [8–11] as models of infinite stepped layer structures of MoO_3 and V_2O_5 crystals, which are used as heterogeneous catalysts in a variety of organic oxidation reactions. Fig. 1 shows the molecular structures of $[\{(\eta^3\text{-}C_4H_7)_2Rh\}_2V_4O_{12}]$ and $[(RhCp^*)_4V_6O_{19}]$ as potential models relevant to metal-supported catalysts having heterometallic centers. They have multifunctional properties and synergetic effects on reactivity owing to the heterometallic centers relevant to metal-supported catalysts whose catalytic activity and selectivity are affected by local metal-supported bondings. We characterized silica-grafted $[(MCp^*)_4Mo_4O_{16}]$ and $[(MCp^*)_4V_6O_{19}]$ (M = Rh, Ir) by EXAFS, FTIR, UV–Vis and TPD, which exhibited high catalytic activities for the olefin hydroformylation and selective oxidation of propene to acetone. We proposed a bifunctional role played by Rh and vanadate/molybdate cluster moieties to promote the selective oxidation of propene and hydroformylation reaction to oxygenates.

The intrazeolite circumstances such as a 'solid-solvent' including acid/base sites, accommodate the selected molecular species and promote the desired organometallic synthetic reactions, similarly to a homogeneous solution. We have synthesized uniformly by the 'ship-in-bottle technique' encapsulated metal carbonyl clusters such as $Rh_4(CO)_{12}$/ALPO-5, $Rh_6(CO)_{16}$/NaY [12–14], $Ir_6(CO)_{16}$/NaY [15,16], $[Pt_3(CO)_3(\mu_2\text{-}CO)_3]_n^{2-}$ (n = 3, 4)/NaY [17,18] and $[Ru_6(CO)_{18}]^{2-}$/NaX [19] and heterometallic $[Fe_2Rh_4(CO)_{15}]^{2-}$/NaY [5] and $Rh_{6-x}Ir_x(CO)_{16}$ (x = 2–4)/NaY [12,20] inside zeolite cages (7–13 Å) and characterized by
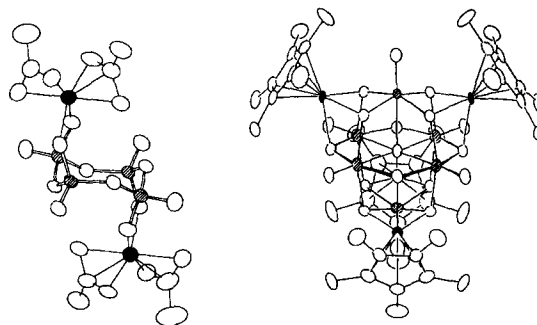

Fig. 1. Left: molecular structure of $[\{\eta^3\text{-}C_4H_7)_2Rh\}_2V_4O_{12}]$, and right: molecular structure of $[(RhCp^*)_4V_6O_{19}]$ as potential models relevant to metal-supported catalysts having heterometallic centers.

EXAFS/XANES, FTIR, ^{129}Xe NMR, HRTEM and Raman spectroscopies. Recently, we synthesized longer rod-like clusters such as $[NR_4]_2[Pt_{15}(CO)_{30}]$ (R = Me, Et, Pr, Bu and Hex) highly ordered in hexagonal mesoporous channels (27.5 Å) of FSM-16, managing uniform distribution of Pt_{15} clusters in a controlled distance by quaternary alkyl amine cations [21]. They are effective as catalysts and hosts for thermostable robust metal/bimetal carbonyl clusters and particles (10–25 Å), which exhibited high activities for the water–gas shift reaction.

In this work, we have conducted the low-temperature homologation of methane on a series of zeolite-entrapped, Ru, Rh, Co and Pt catalysts which were prepared from $Ru_3(CO)_{12}$/NaY, $H_4Ru_4(CO)_{12}$/NaY, $[HRu_6(CO)_{18}]^-$]/NaY, $Co_4(CO)_{12}$/NaY, $Rh_6(CO)_{16}$/NaY, $[Pt_3(CO)_3(\mu_2\text{-}CO)_3]_n^{2-}$ (n = 3)/NaY. The carbon species $[CH_x]$ (x = 0–3) are deposited on naked metal clusters in NaY by admission of methane at 423–623 K, which is completely converted by hydrogen at 300–423 K to C_1–C_5 hydrocarbons without any formation of graphitic carbons. The reactivity of surface carbon bound to metal clusters in zeolites and mechanism for C–C bond formation will be discussed in conjunction with metal/alloy ensemble-size effects and intrazeolitic chemical circumstances.

2. Experimental and procedures

2.1. Catalyst preparation and catalytic reactions

$[n\text{-Bu}_4N]_2[\eta^3\text{-}C_4H_7\}_2Rh\}_2(V_4O_{12})]$ and $[(RhCp^*)_4V_6O_{19}]$ were synthesized and purified by the literature methods [10,11] $(\eta^3\text{-}C_4H_7)_2Rh]_2(V_4O_{12})$ and $[(RhCp^*)_4V_6O_{19}]$ were impregnated at 300 K on SiO_2 (Aerosil 200, Japan Aerosil Co., surface area = 200 m^2/g; dehydrated by evacuation at 573 K). SiO_2 was mixed with the CH_2Cl_2 solution of both cluster compounds, followed by removal of the solvent. The weight loading of the cluster in each sample was 15–20 wt% per supporting silica. The impregnated material was mounted into the microreactor and treated by thermal activation in vacuo or by exposure to 13.3 kPa of O_2 at 353–413 K, resulting in SiO_2-grafted samples, denoted as $Rh_2V_4O_{12}/SiO_2$, (1) and $Rh_4V_6O_{19}/SiO_2$, (2) respectively. The molybdenum oxide cluster compounds such as complete cubane-type $[(RhCp^*)_4Mo_4O_{16})]$ (3) and incomplete $[(RhCp^*)_2Mo_3O_9(OMe)_4]$ (4) were synthesized and purified by the literature methods [8,9]. The impregnated materials were charged into a microreactor and subject to the reduction with CO under the photoillumination, being passed through a color filter to cut-off the > 750 nm infrared region using a ultra-high pressure Hg lamp (Ushio Electric Co., USH-500D), followed by the thermal evacuation to remove CO.

The samples containing 3.2 wt% Ru were prepared by cation-exchange of NaY (LZY-52 from Toso, Si/Al = 5.6) with $Ru(NH_3)_6Cl_3$ aqueous solution at 300 K for 2 days. After filtering and washing with deionized water, the samples were dried at 393 K, which were exposed to a CO + H_2 mixture (200/200 Torr) in a closed circulating reactor by the temperature-programmed heating from 300 to 354–413 K, resulting in $[HRu_6(CO)_{18}]^-/NaY$, with characteristic IR carbonyl bands at 2126(w), 2062(vs), 2044(s), and 1975(s) cm^{-1}. $Co_4(CO)_{12}/NaY$,

with characteristic carbonyl bands at 2126(w), 2078(s) and 1817(m) cm^{-1}, was prepared by the immersion of a NaY pellet in $Co_2(CO)_8$ under atmosphere at 323 K, according to the literature method [22]. The metathesis and oxidation reactions of propene were carried out at 273–323 K using closed circulating systems equipped with a Pyrex glass reactors, whose volumes are 186 and 206 ml, respectively. Products consisting of ethene and 2-butenes were quantitatively analyzed by gas chromatography (Hitachi 163 Type GC) using silica and VZ-10 columns.

2.2. IR, XAFS and TPD studies

Transmission infrared (IR) spectra were obtained from 200 scans at a resolution of 2 cm^{-1} using Shimadzu FTIR-8100M infrared spectrophotometer. The silica-impregnated $Rh_2V_4O_{12}/SiO_2$, (1), $Rh_4V_6O_{19}/SiO_2$, (2), and $[(RhCp^*)_4Mo_4O_{16}]$ (3) were pressed into a self-supporting disc of 40 mg/15 mm diameter, which were mounted in a quartz IR cell.

Rh and Mo(V)–K edge EXAFS (extended X-ray absorption fine structure) spectra were measured for the precursor crystal and silica-impregnated sample before and after CO photoreduction by transmission mode at BL-10B and -7C of the Photon Factory in National Laboratory for High Energy Physics. The spectra were measured by transmission mode and Si(311) channel cut monochrometer was used. The EXAFS spectra were analyzed with a curve-fitting method using the computer program supplied by Technos, with experimental parameters. The backscattering amplitude and phase shift of M–O, M–M and M–Rh (M = V, Mo and Ru) were calculated from Na_2MoO_4 and Mo foil and those of Rh–C, Rh–O and Rh–Metal were evaluated from $Mo(CO)_6$, Na_2MoO_4, Rh and Ru foil, respectively.

Temperature-programmed desorption (TPD) was conducted in evacuating with a ramping rate of 2 K/min from 300 to 573 K. The evolved products were monitored by an Anelva

100A quadruple mass spectrometer interfaced to the TPD apparatus via a three-stage differential pumping system.

3. Results and discussion

3.1. Molecular modeling of supported metal catalysts; SiO_2-grafted $[(\eta^3-C_4H_7))_2Rh]_2V_4O_{12}$ and $[RhCp^*]_4V_6O_{19}$ catalytically active in selective oxidation of propene towards acetone

3.1.1. FTIR / XAFS characterization of surface-grafted Rh capped vanadate clusters

The IR spectra of $[n\text{-}Bu_4N]_2[\{(\eta^3\text{-}C_4H_7)_2Rh\}_2(V_4O_{12})]$ on silica gave bands at 3078 and 3056 cm^{-1} characteristic of the stretching ν(C–H) of $(\eta^3\text{-}C_4H_7)_2$Rh groups capping the precursor cluster, which decreased gradually by increasing evacuation temperature

up to 413 K, along with a considerable suppression of the 3765 cm^{-1} sharp band due to isolated silanol groups on silica support. On the other hand, IR bands at 2990, 2962, 2919, and 2875 cm^{-1} due to ν(CH$_3$/CH$_2$) of counter cation $[n\text{-}Bu_4N]^+$ remained unchanged below 450 K. Similarly, it was found by IR observation that Cp* ligand in $[(RhCp^*)_4V_6O_{19}]$/SiO$_2$ was eliminated partially by thermal evacuation at 423 K and under O$_2$ atmosphere at 373 K.

TPD/mass spectral studies were performed using 0.2 g of the sample such as $[n\text{-}Bu_4N]_2[\{(\eta^3\text{-}C_4H_7)_2Rh\}_2(V_4O_{12})]$/SiO$_2$ and $[Rh(acac)(\eta^3\text{-}C_4H_7)_2]$/SiO$_2$ (acac = acetylacetonate) which were charged in a microreactor and heated by flowing He from 300–600 K with temperature increasing rate is 2 K/min. In the TPD spectra as shown in Fig. 2A and 2B, it was found that 2-methylpropene derived from about a half of $\eta^3\text{-}C_4H_7$ ligands

Table 1

Structural parameters of V K-edge EXAFS for $[n\text{-}Bu_4N]_2[\{(\eta^3\text{-}C_4H_7)_2Rh\}_2(V_4O_{12})]$/SiO$_2$ and $(RhCp^*)_4V_6O_{19}$/SiO$_2$ before and after thermal activation in vacuo and under O$_2$ atmosphere

Sample	Absorption/back-scattering	C.N. [a]	R/Å [b]	R factor/%
$[n\text{-}Bu_4N]_2[\{(\eta^3\text{-}C_4H_7)_2Rh\}_2(V_4O_{12})]$/BN	V=O	1.0	1.65	13.3
	V–O	3.0	1.82	
$[n\text{-}Bu_4N]_2[\{(\eta^3\text{-}C_4H_7)_2Rh\}_2(V_4O_{12})]$/SiO$_2$ impregnation	V=O	1.2	1.65	7.2
	V–O	3.7	1.84	
after evacuation at 413 K	V=O	1.0	1.64	6.5
	V–O	3.1	1.84	
exposure to O$_2$ at 413 K	V=O	1.0	1.64	15.4
	V–O	3.3	1.83	
exposure to O$_2$ at 523 K	V=O	0.7	1.65	10.4
	V–O	2.1	1.84	
$(RhCp^*)_4V_6O_{19}$/BN	V=O	1.0	1.62	
	V–O$_b$	4.0	1.88	5.2
	V–O$_c$	1.0	2.31	
$(RhCp^*)_4V_6O_{19}$/SiO$_2$ impregnation	V=O	1.0	1.60	
	V–O$_b$	4.0	1.88	8.3
	V–O$_c$	2.2	2.29	
after evacuation at 373 K	V=O	1.2	1.62	
	V–O$_b$	3.5	1.86	4.2
	V–O$_c$	1.2	2.28	

[a] C.N.: Normalized coordination number.

[b] R/Å = interatomic distance.
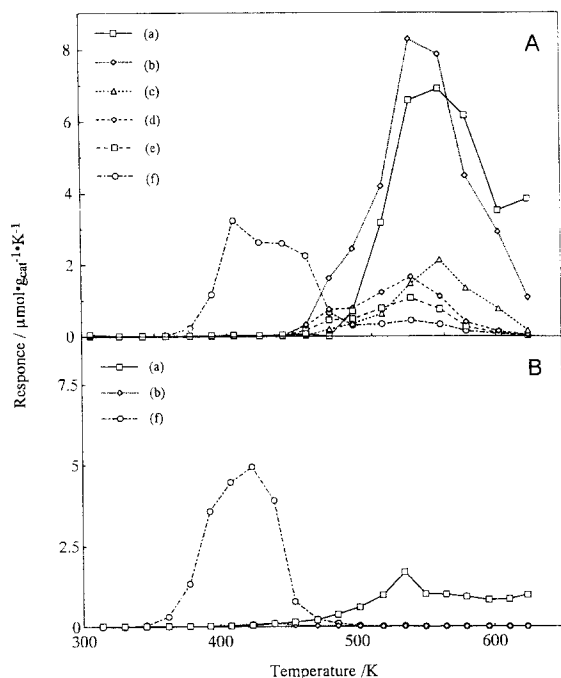
Fig. 2. TPD patterns of (A) [n-Bu$_4$N]$_2$[{η^3-C$_4$H$_7$)$_2$Rh}$_2$(V$_4$O$_{12}$)] and (B) [Rh(acac)(η^3-C$_4$H$_7$)$_2$] impregnated on SiO$_2$ gel. Yields of (a) 2-methylpropene, (b) methane, (c) propane, (d) butane, (e) trans-2-butene, and (f) cis-2-butene.

bound to Rh$_2$V$_4$O$_9$ and Rh (acac) moieties on silica was evolved at 350–413 K and all of them completely desorbed below 450 K. Other species such as CH$_4$, C$_3$H$_6$ and 2-butenes were formed on [n-Bu$_4$N]$_2$[{(η^3-C$_4$H$_7$)$_2$Rh}$_2$(V$_4$O$_{12}$)]/SiO$_2$ (Fig. 2A) at higher temperatures above 450 K, resulted from Hoffman degradation of [n-Bu$_4$N]$^+$.

The Fourier transform (FT) peaks of Rh–C and Rh–O contribution were obtained from the raw Rh edge EXAFS data for [n-Bu$_4$N]$_2$[{(η^3-C$_4$H$_7$)$_2$Rh}$_2$(V$_4$O$_{12}$)]/SiO$_2$ with a k^3-weighting over the range 3.5 < k < 15 Å^{-1}. When the sample was evacuated at 413 K, intensity of the Rh–C peak decreased ($R = 2.17$ Å, C.N. = 3.2) by half of that in the precursor sample ($R = 2.19$ Å, C.N. = 5.6), whereas the C.N. of Rh–O ($R = 2.07$ Å) bonding in the precursor sample increased relatively from 1.8 to 2.1, possibly due to surface-attachment of capped η^3-C$_4$H$_7$)$_2$Rh with silanol groups. Table 1 shows structural parameters for k^3 weighted V–K edge EXAFS of Rh$_2$V$_4$O$_{12}$/SiO$_2$, (1) and Rh$_4$V$_6$O$_{19}$/SiO$_2$, (2) before and after the thermal activation in vacuo or O$_2$ atmosphere of 13.3 kPa. When the sample (1) was evacuated at 300–413 K, the intensity and shape of the FT peaks of V=O and V–O remained unchanged, which agree well with those of the precursor cluster e.g. [n-Bu$_4$N]$_2$[{η^3C$_4$H$_7$)$_2$Rh}$_2$(V$_4$O$_{12}$)] in the crystalline state. When the sample (1) was evacuated at 513 K, the resulting FT spectra changed substantially, resembling that of conventional V$_2$O$_5$/SiO$_2$ which was prepared by calcination of ammonium vanadate on silica. Accordingly, the results of FTIR, EXAFS and TPD studies suggest that chair-form vanadate tetramer and hexamer clusters capped with (η^3-C$_4$H$_7$)$_2$Rh and RhCp* groups were grafted with Rh end on silica surface, as depicted in Scheme 1; in keeping the vanadium oxide (V$_4$O$_{12}$ and V$_6$O$_{19}$) cluster frameworks basically unchanged,
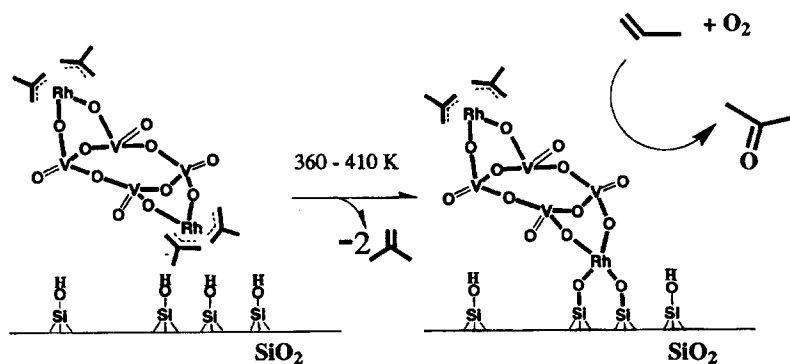
Scheme 1.

at least by thermal activation in vacuo or under the oxygen atmosphere below 413 K.

A gas mixture of propene (13.3 kPa) and oxygen (13.3 kPa) was admitted to the samples of $Rh_2V_4O_{12}/SiO_2$, (1) and $Rh_4V_6O_{19}/SiO_2$, (2). It was of interest to find that although propene oxidation occurred negligibly on both Rh-capped vanadium oxide cluster compounds in crystal, acetone was produced catalytically in keeping higher selectivities (43–85% mol) on $Rh_2V_4O_{12}/SiO_2$, (1) and $Rh_4V_6O_{19}/SiO_2$, (2) after grafted on silica surface. As shown in Table 2, by exceeding the activation temperature at 513 K, the catalytic activity and selectivity for acetone formation decreased substantially, possibly due to the degradation of Rh capped vanadate clusters. For the Arrhenius plots in propene oxidation on $Rh_2V_4O_{12}/SiO_2$, the activation energies were obtained as 46.8 kJ/mol for acetone production, 35.5 kJ/mol for CO_2 production, respectively. As shown in Table 2, the $Rh_4V_6O_{19}/SiO_2$, (2) exhibited higher selectivities towards acetone rather than $Rh_2V_4O_{12}/SiO_2$ (1). By contrast, the oxidation of propene to acetone gave poor selectivities and conversion with higher activation energy of 73.7 kJ/mol over $Rh(acac)(\eta^3\text{-}C_4H_7)_2/SiO_2$. By contrast, a negligible amount of acetone was obtained in the reaction on $[V_{10}O_{28}]/SiO_2$ derived from non-Rh capped vanadate dodecamer cluster $[(n\text{-}Bu)_4]_2(V_{10}O_{28})$ and the conventional V_2O_5/SiO_2 under the similar reaction condi-

tions. The results suggested that the coordinately unsaturated Rh site capped with vanadium oxide cluster frameworks are associated with the selective catalysis for propene oxidation to give acetone.

As recently reported by Minoum et al. [22,23], allyl Rh complexes catalysed the selective oxidation of 1-olefin to 2-ketone in solution, the activity of which was retarded strongly with water. Actually, it was found that acetone formation in propene oxidation on $Rh_2V_4O_{12}/SiO_2$, (1) and $Rh_4V_6O_{19}/SiO_2$ (2) was not affected or rather suppressed by the addition of water. The results indicate that this reaction was not Wacker-type likely on the conventional binary acidic Mo–Co oxides and redox-cycle catalyzed by $CuCl_2$–$PdCl_2$ in solution. By contrast, acetone is formed by the reaction mechanism directly between propene and O_2 through a peroxy intermediate. Schwarz et. al. [24] recently also reported that acetone was formed with higher selectivities on the surface-grafted Rh derived from $Rh(\pi\text{-allyl})_3$ impregnated on Al_2O_3.

3.2. CO-photoreduced cubane–molybdenum oxide clusters as molecular modeling of oxygen-deficient MoO_3 catalytically active for propene metathesis reaction

The triple cubane-type structure of $[(RhCp^*)_4Mo_4O_{16}]$ (3) is a linear structure

Table 2
Catalytic performance of SiO_2 grafted vanadate tetramer and hexamer capped with Rh and other impregnated materials

Catalyst	Formation of acetone in propene oxidation			
	TOF s^{-1}	Selectivity [a] mol%	Activation energy [b]/kJ · mol^{-1} acetone	CO_2
$[n\text{-}Bu_4N]_2[\{(\eta^3\text{-}C_4H_7)_2Rh\}_2(V_4O_{12})]_2/SiO_2$	2.3×10^{-6}	41	47	36
$(RhCp^*)_4V_6O_{19}/SiO_2$	1.7×10^{-6}	85	45	62
$Rh(acac)(\eta^3\text{-}C_4H_7/SiO_2$	0.6×10^{-6}	13	74	29
$[n\text{-}Bu_4N]_3(V_{10}O_{28}H_3)/SiO_2$	0.1×10^{-6}	54	–	–
V_2O_5/SiO_2	$< 10^{-8}$	≈ 0	–	–

$P_{C_3H_6} = P_{O_2} = 13.3$ kPa. Reaction temperature: 343 K.
[a] Selectivity for acetone.
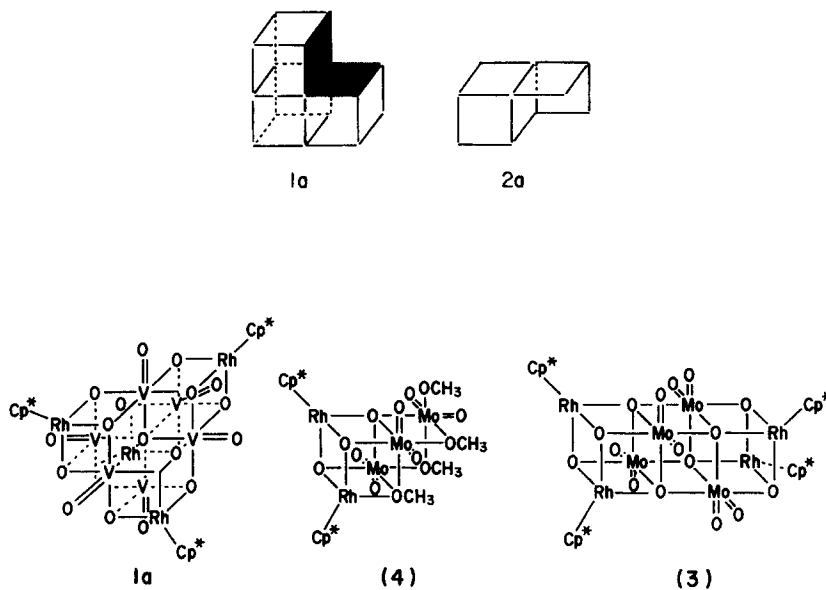[b] Activation energy for acetone and CO_2 formation.

Fig. 3. Molecular structure of complete cubane-type [(RhCp*)$_4$Mo$_4$O$_{16}$] (3) and incomplete [(RhCp*)$_2$Mo$_3$O$_9$(OMe)4] (4) simple drawing.

compound where complete cubic units fuse together by sharing faces, as shown in Fig. 3. These oxide clusters capped with Rh and Ir ligands have gained attention as molecular modeling of the supported metal catalysts. On the other hand, the [(RhCp*)$_4$Mo$_4$O$_{16}$] reacts with MeOH in the presence of p-hydroquinone to produce incomplete double cubane-type cluster [(RhCp*)$_2$Mo$_3$O$_9$(OMe)$_4$] (4) which has a cluster framework characteristic of the ordered MoO$_3$(100) face (2a), which is highly active in the oxidation of methanol and propene. In Fig. 3, an incomplete cubane–Mo oxide cluster (1a) is represented as a molecular modeling of oxygen-deficient site located at MoO$_3$(111) crystal steps.

3.2.1. Photoreduction of Rh capped cubane–Mo$_4$O$_{16}$ and Mo$_3$O$_9$ clusters in CO

Prolonged photoreduction of [(RhCp*)$_4$Mo$_4$O$_{16}$]/SiO$_2$ (3) was performed under CO at 300 K with the mercury lamp, proving about 2.5–3 moles of CO$_2$ per one mole of the Mo$_4$ oxide cubane cluster. There are two sets of the intense IR bands (2092, 2035 cm^{-1} and 2061, 2021 cm^{-1}), as presented in Fig. 4(a). It was found that the latter peaks at 2061 and 2021 cm^{-1} are substantially suppressed and eventually disappeared in a thermal evacuation at 373–423 K. Whereas, the other two peaks at 2092 and 2035 cm^{-1} are thermally stable. The latter peaks are facile for ^{13}CO exchange reaction at 300 K, and exhibited the isotopic band-shift towards 2043 and 1987 cm^{-1} (Fig. 4(b)). The former CO stretch bands at 2061 and 2021 cm^{-1} are thermally inactive for the exchange reaction at 300 K, but readily exchanged with ^{13}CO under Hg lamp irradiation at 300 K: the IR bands shifted to 2013 and 1974 cm^{-1}, respectively, as shown in Fig. 4(c). By comparison, there are some referred IR data for some Rh carbonyl species such as [Rh(CO)$_2$Cl]$_2$ (ν_{CO} = 2095 and 2045 cm^{-1}), and surface-grafted Rh(CO)$_2$ (ν_{CO} = 2104–2085 and 2042–2035 cm^{-1}) derived from Rh$_4$(CO)$_{12}$ impregnated on SiO$_2$ and Al$_2$O$_3$. They are exchanged with ^{13}CO at 300–423 K [25]. In addition, Ekardt et al. [26] reported that the molybdenum carbonyl species are formed by ultraviolet photoreduction of MoO$_3$/SiO$_2$ in CO, showing the twin CO stretch bands at 2128 and 2080 cm^{-1} due to the tetrahedral Mo(IV)(CO)$_2$ species.

Accordingly, it was proposed that the two sets of CO stretch bands are associated with CO attached to Rh and Mo atoms in the photoreduced $(RhCp^*)_4Mo_4O_{16}]/SiO_2$ (3) in CO, respectively. FTIR and TPD study suggested that all of CO on the samples produced by the photo-CO reduction was eliminated at 330–440 K, leaving the oxygen-deficient Mo sites in the cubane–oxide cluster attached with silica.

In order to obtain more structural information about the CO-photoreduction of the molybdenum oxide clusters (3) and (4), EXAFS measurements was carried out. Fig. 5 presents the raw EXAFS function and the Fourier Transform
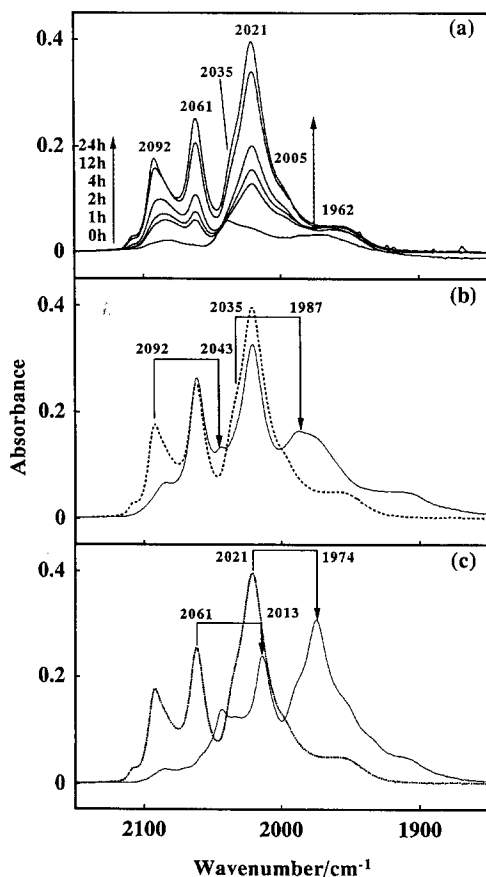
Fig. 4. IR spectral changes of (a) SiO_2-impregnated complete cubane-type $[(RhCp^*)_4Mo_4O_{16}]$ (I) in CO (1.33 kPa) under the Hg-lamp illumination at 300 K for 0–24 h, (b) after the exposure of ^{13}CO (1.33 kPa) at 300 K to the CO-photoreduced sample (a), and (c) under Hg-lamp illumination with exposure of ^{13}CO (1.33 kPa) at 300 K.

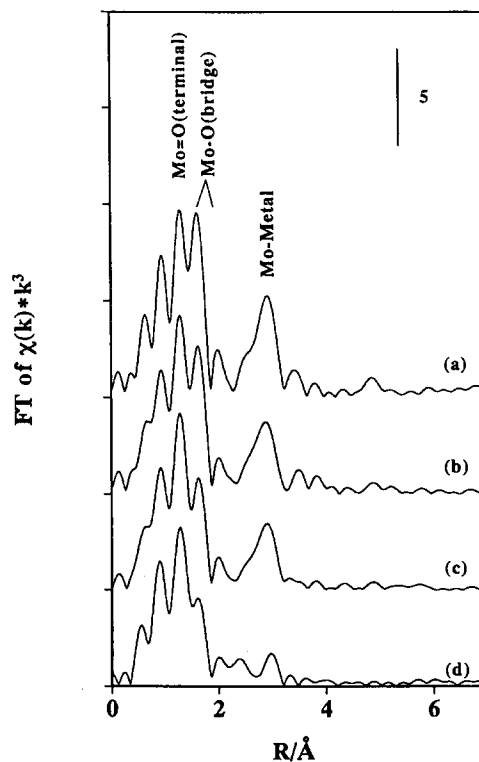Fig. 5. Fourier-transformed Mo–K edge EXAFS oscillation $(\chi(k)^* k^3)$ of SiO_2-impregnated complete cubane-type $[(RhCp^*)_4Mo_4O_{16}]$ (I) (a) $[(RhCp^*)_4Mo_4O_{16}]/BN$ (boron nitride) (b) $[(RhCp^*)_4Mo_4O_{16}]/SiO_2$, (c) after photoreduction in CO (13.3 kPa) at 300 K for 24 h (d) after evacuation of the sample (c) at 473 K for 2 h.

(FT) for silica-supported $[(RhCp^*)_4Mo_4O_{16}]$ (3) sample. The raw EXAFS function [Fig. 5(a)] shows oscillation up to $k = 14$ Å^{-1}, clearly indicating the presence of near-neighbor high atomic weight backscatters, which are inferred to be Mo and Rh. Fig. 6 presents k^3 weighted Mo K edged EXAFS function $(\chi(k)^* k^3)$ of $[(RhCp^*)_4Mo_4O_{16}]$ (3) sample after being evacuated at 300 K. The Mo–O contribution in the precursor (3) are reasonably resolved in three Mo–O bonds with different bond length denoted as $Mo=O_{(terminal)}$ ($R = 1.72$ Å, C.N. = 2.0), $Mo-O_{3c(bridge)}$ ($R = 1.93$ Å, C.N. = 2.0) and $Mo-O_{4c(bridge)}$ ($R = 2.32$ Å, C.N. = 2.0), respectively. In addition, the Mo–Rh ($R = 3.28$ Å, C.N. = 2.0) and Mo–Mo ($R = 3.36$ Å, C.N. = 3.0) bondings were detected in the secondary coordination sphere. Table 3 lists the

results of the data analysis for the silica-supported $[(RhCp^*)_4 Mo_4O_{16}]/SiO_2$ before and after CO-photoreduction and thermal evacuation of the resulting material. The Mo–K edge EXAFS data suggested that the 4c-bridged Mo–O bond contribution was specifically suppressed ($R = 1.94$ Å, C.N. $= 0.4$) compared with those of the other Mo–O bonds after the CO-photoreduction. It is interesting to find that according to the Rh–K edge EXAFS data for these samples, the Rh–O (4c) bond contribution of the triple cubane $[(RhCp^*)_4Mo_4O_{16}]/SiO_2$ was clearly decreased by the photoillumination under CO atmosphere, compared with those of the Rh–O (3c) and Rh–C. The subsequent thermal evacuation at 473 K to remove CO from the carbony-

Table 3

EXAFS results for (a) $[(RhCp^*)_4Mo_4O_{16}]$ (I) diluted in boron nitride (BN) crystal, (b) (I) impregnated on SiO_2 after evacuation at 300 K, (c) after photoreduction of the sample (b) in CO (13.3 kPa) at 300 K for 24 h and (d) after evacuation of the sample (c) at 473 K for 2 h to remove CO

	Samples	Bond	$R/$Å [a]	C.N.	$\Delta E_0/$eV	$\Delta\sigma/$Å	R factor/%
(a)	$(RhCp^*)_4Mo_4O_{16}/BN$	Mo=O(terminal)	1.73 (1.70)	2.0	1.9	0.000	7.98
		Mo–O(3c(bridge))	1.94 (1.93)	2.0	1.9	0.001	
		Mo–O(4c(bridge))	2.39 (2.34)	2.0	1.9	0.000	
		Rh–O(bridge)	2.11 (2.10)	3.0	−1.4	0.034	6.18
		Rh–C	2.15 (2.13)	5.0	−5.4	0.056	
		Mo–Metal(Mo)	3.28 (3.22)	2.0	−4.5	0.001	7.55
		Mo–Metal(Rh)	3.37 (3.36)	3.0	−2.3	0.000	
		Rh–Metal(Rh)	3.28 (3.33)	1.0	−4.2	0.006	8.55
(b)	$(RhCp^*)_4Mo_4O_{16}/SiO_2$	Mo=O(terminal)	1.73	1.9	2.1	0.000	5.14
	(evacuation at 300 K)	Mo–O(3c(bridge))	1.94	1.7	2.1	0.020	
		Mo–O(4c(bridge))	2.40	1.8	2.1	0.032	
		Rh–O(bridge)	2.10	2.8	−2.8	0.037	5.97
		Rh–C	2.15	4.6	−5.0	0.050	
		Mo–Metal(Mo)	3.27	1.9	−3.7	0.000	9.34
		Mo–Metal(Rh)	3.38	2.6	−4.2	0.000	
		Rh–Metal(Rh)	3.21	0.7	−7.2	0.005	2.19
(c)	$(RhCp^*)_4Mo_4O_{16}/SiO_2$	Mo=O(terminal)	1.73	1.9	1.9	0.000	6.74
	(photoreduction in CO)	Mo–O(3c(bridge))	1.94	1.7	1.9	0.042	
		Mo–O(4c(bridge))	2.41	1.3	1.9	0.001	
		Rh–O(bridge)	2.10	2.4	−2.3	0.027	4.31
		Rh–C	2.17	5.0	−3.4	0.076	
		Mo–Metal(Mo)	3.28	1.7	−3.2	0.000	8.87
		Mo–Metal(Rh)	3.38	2.3	−3.6	0.000	
		Rh–Metal(Rh)	–	–	–	–	
	(d) $(RhCp^*)_4Mo_4O_{16}/SiO_2$	Mo=O(terminal)	1.72	1.6	0.47	0.001	6.96
	(evacuation at 473 K after CO-photoreduction)	Mo–O(3c(bridge))		1.95	1.5	0.47	0.060
		Mo–O(4c(bridge))	2.45	1.1	0.47	0.016	
		Rh–O(bridge)	2.12	1.9	−1.1	0.048	3.70
		Rh–C	2.19	5.4	−3.1	0.080	
		Mo–Metal(Mo)	3.25	1.8	−2.8	0.108	10.16
		Mo–Metal(Rh)	3.33	1.4	−2.0	0.037	
		Rh–Metal(Rh)	–	–	–	–	

C.N., $R/$Å, $E_0/$eV and $\Delta\sigma/$Å, represent coordination number, interatomic distance, changes in inner potential correction and Debye–Waller factor, respectively.
[a] Distances in parentheses are from X-ray crystal structure data (Ref. [4]).
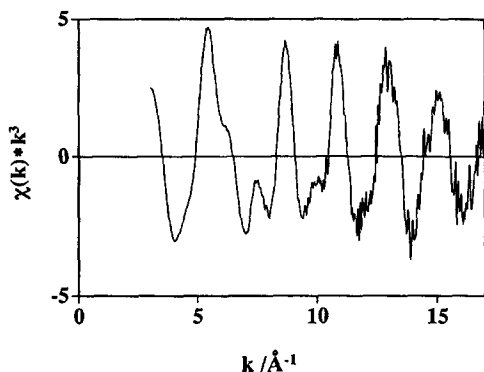
Fig. 6. k_3 weighted Mo-K edge EXAFS function ($\chi(k)^* k_3$) of [(RhCp*)$_4$Mo$_4$O$_{16}$]/SiO$_2$ evacuated at 300 K.

Fig. 7. Product formation in propene metathesis reaction at 300 K on the CO-photoreduced complete cubane-type [(RhCp*)$_4$Mo$_4$O$_{16}$] (I) and incomplete [(RhCp*)$_2$Mo$_3$O$_9$(OMe)$_4$] (II) after the thermal evacuation at 473 K.

lated sample resulted in the further decrease of C.N. for 4c-bridge Mo–O (4c), Rh–O (4c) and Mo–Rh as well as Mo–Mo bonds, followed by a slight elongation of the interatomic distances, as shown in Table 3. The results suggest that the bridging Mo–O (4c) and Rh–O (4c) were selectively reduced by CO-photoreduction in keeping the triple cubane cluster framework. Kazansky [27] previously proposed a model for the photoreduction of MoO$_3$/SiO$_2$ catalyst in CO which proceeds the removal of terminal Mo(VI)=O bond to give Mo(IV) and CO$_2$.
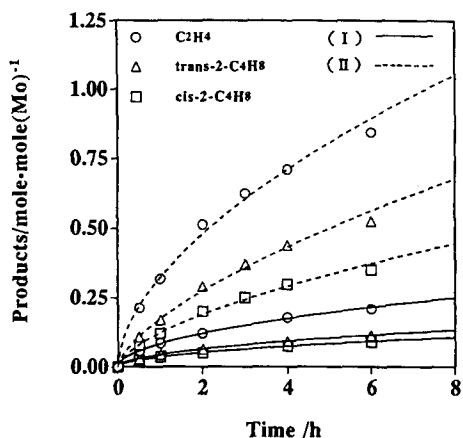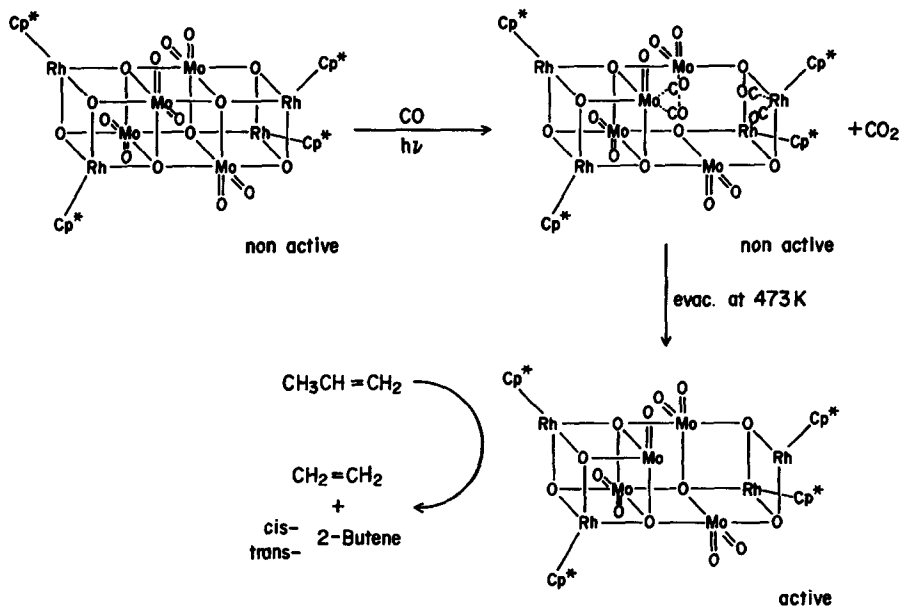
EXAFS, FTIR and TPD results in this work suggested that the 4c bridged Mo–O bonds, whereas a negligible removal Mo(VI)=O bond, are selectively reduced under the photoillumination in CO, resulting in the formation of the carbonyls attached to Rh and Mo sites in the distorted cubane-type cluster frameworks. The

Scheme 2. Proposed structures of CO-photoreduced (RhCp*MoO$_4$)$_4$/SiO$_2$.

further removal of CO eventually led to the formation of oxygen deficient Mo(IV)/Mo(V) sites with coordinative unsaturation.

3.2.2. Propene metathesis reaction

Propene (100 Torr) was admitted to the samples of (3) and (4) after the CO-photoreduction at 300 K followed by thermal evacuation at 473 K (Fig. 7). Both precursor samples of SiO_2-impregnated triple cubane-type $[(RhCp^*)_4Mo_4O_{16}]$ (3) and incomplete $(RhCp^*)_2Mo_3O_9(OMe)_4$ (4) were inactive for the propene metathesis reaction. The reaction negligibly proceeded even after the CO-reduction under the photoillumination. It was demonstrated that the CO-photoreduced samples (3) and (4) after the thermal evacuation at 423–473 K exhibited marked activities for the propene metathesis at 273–323 K to make an equimolar mixture of ethene and 2-butenes. As shown in Fig. 8, the incomplete cubane-type Mo oxide cluster (4) exhibited over 3 times higher activities for the propene metathesis than the complete cubane (3). The CO-photoreduced com-

plete cubane (3) sample had a much larger activation energy ($E_a = 11.2$ kJ/mol) than the incomplete cubane (4)-derived one ($E_a = 4.8$ kJ/mol) under the similar reaction conditions. Furthermore, it is noteworthy that the trans/cis molar ratios of the produced 2-butenes on the former catalyst (4) (trans/cis = 1.7) is higher than the ratio on the (3) (trans/cis = 1.3). This may suggest that the oxygen-deficient Mo active sites prepared by the CO-photoreduction offer preferable formation of trans-2-butene via a more sterically crowded metallocyclic intermediate for the propene metathesis reaction than those in the incomplete Mo_3 cubane moiety as suggested in Scheme 2, where the oxygen-deficient sites are induced by CO photoreduction of cubane-type Mo oxide clusters.

3.3. Ship-in-bottle synthesis of Ru carbonyl clusters in NaY zeolite and their XAFS/FTIR characterization

$Ru_3(CO)_{12}$ in NaY (4 wt% Ru) designated as $Ru_3(CO)_{12}$ prepared by vapor deposition at
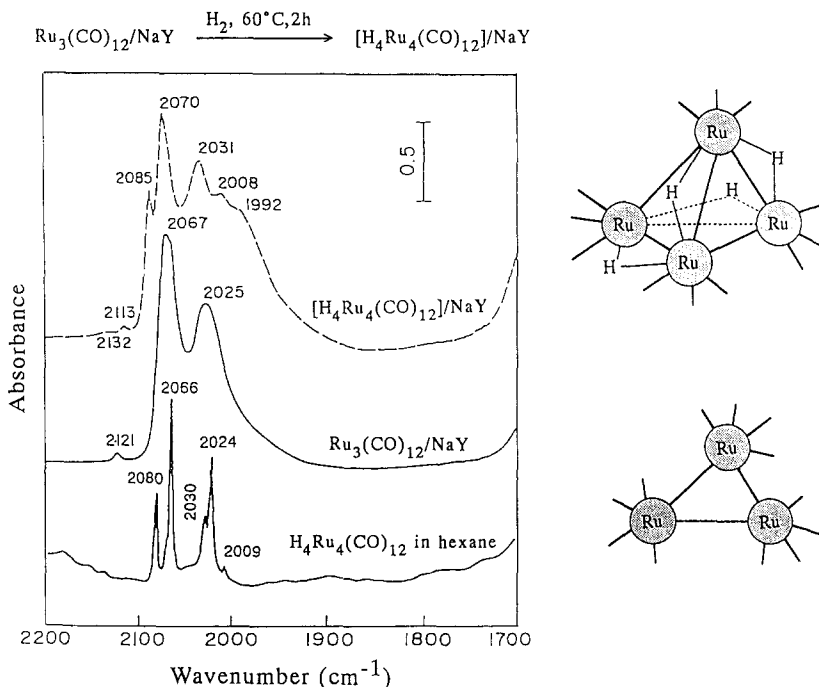

Fig. 8. In situ FTIR spectra in the reaction of $Ru_3(CO)_{12}$ encapsulated in NaY pores with H_2 (200 Torr) at 298–363 K; reference spectrum of $H_4Ru_4(CO)_{12}$ in hexane solution, (b) initial spectrum of $Ru_3(CO)_{12}/NaY$ in vacuo, 238 K, (c) 363 K, 2 h.

323–363 K, showing the characteristic IR carbonyl bands (ν_{CO} = 2124(w), 2068(s), 2028(s) cm^{-1}; diffused reflectance UV–Vis, 234, 392 nm). About 1.0 g of NaY crystals (LZY-52 from Toso, Si/Al = 2.8, surface area 910 m^2) was evacuated in vacuo at 673 K to remove water, which was mixed with $Ru_3(CO)_{12}$ crystal (Strem, 99.% purified from n-hexane solution) under nitrogen atmosphere. The mixed sample in a sealed Pyrex glass tubing was heated at 354 K for 4 days, where sublimation of $Ru_3(CO)_{12}$ on to NaY proceeded without concomitant evolution of carbon monoxide. The XRD (X-ray diffraction, Cu-K α) patterns suggests that the crystalline phase of $Ru_3(CO)_{12}$ at 2θ = 12.60, 16.44, and 30.42) mixed with NaY zeolite completely disappeared after the thermal treatment at 354 K, leaving only those of NaY crystals (2θ = 6.28, 10.2, 11.96, 15.72, 18.72, 20.44, 21.34, 23.72, 27.84, 30.82, 31.48). The Ru contents of the aging samples were determined, by using an inductively coupled plasma–atomic emission (ICP) spectrometer, to be 4.3 wt% Ru loading which was invariant before and after heat treatment of the mechanical mixture. This suggests that a gaseous $Ru_3(CO)_{12}$ (6–7 Å Van der Waals radius) is diffused into and highly dispersed in the zeolite micropores through the apertures of the cages (7.4 Å) by spontaneous monolayer dispersion [6]. As shown in Fig. 8, the IR spectra of the resulting sample gave intense bands at 2066(s) and 2030(s) cm^{-1}, which strongly resemble those of $Ru_3(CO)_{12}$ (2060(s), 2026(s) and 2002(m) cm^{-1}) in crystal and hexane solution. It is noteworthy that the stretching frequency of terminal ν_{CO} is slightly blue-shifted by 5–10 cm^{-1} with respect to those of external $Ru_3(CO)_{12}$. The diffuse reflectant UV–Vis spectra were measured for the physical mixture of $Ru_3(CO)_{12}$ and NaY before and after the thermal aging for 4 days at 354 K, showing the bands at 234 and 320 nm. The resulting orange-colored material was very reactive with H_2 (100–400 Torr) using a closed circulating system by removal of a trace of water with a liquid N_2 trap at 323–363 K led to the forma-

tion of hydridocarbonyl cluster in NaY as the analogy to the reaction in hexane;

$$Ru_3(CO)_{12}/NaY + H_2 \rightarrow H_4Ru_4(CO)_{12}/NaY,$$

giving the bands at 2082(m), 2064(s), 2032(m), 2021(m) and 2001(w) cm^{-1}, which resemble those of $H_4Ru_4(CO)_{12}$ in cyclohexane solution (ν_{CO} = 2081(m), 2067(s), 2031(m) and 2024(m) cm^{-1}; UV–Vis 230 and 390 nm). By analogy, the bands below 240 nm due to metal–CO CT transition, and the bands in the range of 350–400 nm possibly due to Ru–Ru bonding in the Ru_4 cluster frameworks. To obtain more insight into the structure of Ru carbonyl clusters formed in NaY zeolites, the EXAFS spectra of Ru–K edge were measured for the samples of $Ru_3(CO)_{12}/NaY$ (**I**) and $H_4Ru_4(CO)_{12}/NaY$ (**II**) under N_2 atmosphere at 300 K. The Ru foil, $Ru_3(CO)_{12}$ and $H_4Ru_4(CO)_{12}$ crystals mixed with boron nitride (BN) were used as the references for Ru–Ru and Ru–CO shell. The raw EXAFS data and associated Fourier transforms of the products formed in the H_2-reduction of $Ru_3(CO)_{12}/NaY$ were collected. The results of the curve-fitting analysis are listed in Table 4. With these parameters, a best estimate for the Ru–Ru shell with a Debye–Waller factor of 0.04–0.0099 relative to Ru foil) was deter-

Table 4
Curve fitting results of Ru K-edge EXAFS data [a]

| Sample	Backscattering shell	C.N.	R/Å	ΔE/eV	σ/Å
Ru foil	Ru–Ru	12	2.67	−4.06	0.053
$Ru_3(CO)_{12}$/BN	Ru–Ru	2	2.86	0.35	0.062
	Ru–C	4	1.93	0.88	0.054
	Ru–O	4	3.02	1.11	0.063
$Ru_3(CO)_{12}$/NaY	Ru–Ru	2	2.86	0.46	0.063
	Ru–C	3.8	1.93	1.76	0.053
	Ru–O	3.9	3.00	−1.59	0.053
$Ru_4H_4(CO)_{12}$/NaY	Ru–Ru	3.2	2.80	9.00	0.079
	Ru–C	2.6	1.87	−3.15	0.060
	Ru–O	2.5	3.07	−9.90	0.040
$Ru_6(CO)_{18}^{2-}$/NaX	Ru–Ru	3.5	2.82	12.85	0.060
	Ru–C	3.1	1.86	−6.67	0.060

[a] C.N., R, ΔE and σ represent coordination number, interatomic distance, change in energy threshold and Debye–Waller factor, respectively.

mined, which gave the best agreement with the EXAFS data in r space 2.0–3.8 Å (before the phase-shift correction). The Fourier transform for the sample of (I) is very similar to that of the reference $Ru_3(CO)_{12}/BN$. The interatomic distances and C.N. of both Ru–Ru and Ru–CO bondings are quite consistent between them within the experimental errors ($R = 0.003$ Å and C.N. = 0.2). The results for the sample (II) suggested that Ru carbonyl clusters alike $H_4Ru_4(CO)_{12}$ are most likely formed by H_2 reduction at 365 K inside NaY.

The cluster-impregnated samples such as SiO_2-grafted and zeolite-encaged Ru, Co and Pt carbonyl clusters after removal of the solvents were subjected to the thermal evacuation at 423 K for 2 h, followed by the reduction in H_2 flow (1 bar, 40 ml/min) at the programmed temperature from 293 to 573 K for 2 h and 573 K for 2 h. The sample was transferred to a microreactor and reduced again in H_2 flow at 573 K for 1 h prior to introducing syngas for CO hydrogenation.

3.3.1. Methane homologation on Ru, Co and Pt clusters encapsulated in NaY micropores

A pulse of 0.5% methane diluted in a He flow (40 ml/min) was exposed to the H_2 reduced Ru_3/NaY, Ru_4/NaY, Ru_6/NaY and Ru (50 Å) on NaY (3.2 wt% loading), Co_4/NaY (5 wt%) and Pt_{12}/NaY (5.2 wt%) in a plug flow microreactor. Using a flow-mode reactor of pulse feed of methane, the deposition of methane proceeded at lower temperatures above 323–723 K on these zeolite-entrapped metal cluster catalysts, resulting in the formation of carbonaceous species $[CH_x]$ ($x = 0$–3) with the coverage of $\theta_C = 0.05$–0.67 (C/M). After methane deposition the catalyst was cooled below 300 K to avoid aging ('coking and graphitization'), the surface–carbon species was hydrogenated by a flow of H_2 in ramping the temperatures from 300 K to 873 K. Scheme 3 represents the possible steps of methane homologation towards lower alkanes on the naked Ru clusters in NaY supercages which are derived from

$$2\,CH_4 \; \overset{\longrightarrow}{\longleftarrow} \; C_2H_6 + H_2$$

Scheme 3.
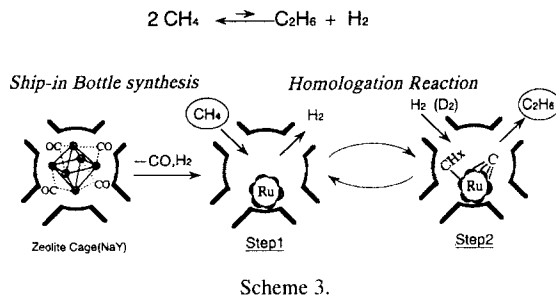
$HRu_6(CO)_{18-}$ synthesized in NaY by ship-in-bottle technique.

Adsorption of methane with hydrogen evolution on the metal clusters in zeolites proceeded at lower temperatures above 323 K with these metal clusters in zeolites, giving the coverage of CH_x species ([C]/M = 0.05–0.38). CH_4 reacts at 423–523 K with $[Co_4]/NaY$ and $[Ru_4]/NaY$ to give CH_x ($x = 2$–3), giving the IR bands (ν_{C-H}) at 2960–2987, 2840–2885 cm^{-1} and those (ν_{C-D}) at 2084, 2048 cm^{-1} for CD_4 on Ru_6/NaY at 523 K, respectively. It is interesting to find that the carbon species $[CH_x]$ was highly active and completely converted with H_2 to C_1–C_5 hydrocarbons, consisting of C_α and C_β with a negligible amount of C_γ as shown in Fig. 9.

By contrast, the TPR pattern on the conventional Ru/Al_2O_3 [28] and Ru (50 Å) on NaY provided TPR patterns with a considerable amount of C_γ which is connected with hydrogen only to methane at high temperatures above 723 K. The surface carbon by methane decomposition below 423 K on $[Ru_3]/NaY$ and $[Ru_6]/NaY$ was almost quantitatively converted with hydrogen towards C_1–C_5 hydrocarbons, and the results are presented in Fig. 10. It is of interest to find the Ru catalysts derived from the carbonyl clusters in NaY exhibited remarkable high activities and selectivities for lower hydrocarbon formation, in particular to form C_2H_6, compared the conventional Ru/Al_2O_3 and Co_4/NaY. The yields of C_2^+ hydrocarbons relatively increased on the Ru catalysts derived from carbonyl clusters in NaY by the following
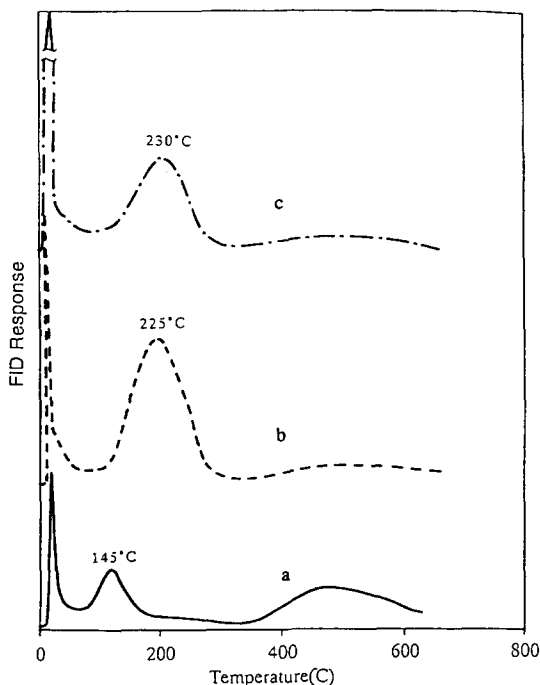
Fig. 9. TPR (temperature programmed reduction) profiles of surface carbon species formed by methane deposition at 623 K on (a) Ru catalyst (C.N. = 11; 50 Å) derived from $Ru_3(CO)_{12}$ /NaY calcined at 423 K for 2 h, followed with H_2 reduction at 623 K; $\theta_C = 0.15$, (b) Ru catalyst (C.N. = 6.7; 10 Å) derived from $Ru_3(CO)_{12}$ /NaY evacuated at 423 K for 2 h, followed with H_2 reduction at 623 K; $\theta_C = 0.25$, and (c) $\theta_C = 0.34$ for (b) sample.

order: $Ru_3/NaY < Ru_4/NaY < Ru_6/NaY < Ru$ (50 Å) on NaY. Increasing the carbon coverage θ_C in methane deposition on

Ru_3/NaY and Ru_4/NaY resulted in the effective enhancement of C_2^+ hydrocarbons consisting of C_2–C_3 alkanes. Ethane was produced in high selectivities (> 90%) among the C_2^+ hydrocarbons in methane homologation on Ru_3/NaY and Pt_{12}/NaY. To provide insight into the mechanism of C–C bond formation and the reactivity of surface carbon bound to Ru clusters in NaY, a pulse feed of D_2 instead of H_2 was admitted to Ru_3/NaY predeposited with CH_4 at 623 K and products in the effluent gas were analyzed by GC/mass spectrometry. As shown in Fig. 11, multi-deuterated methane ($CD_{4-x}H_x$; $x = 0$–2) and fully-deuterated C_2 and C_3 fractions were obtained, implying that C–C propagation proceeded in methane deposition by removal of hydrogen. The removal of hydrogen by methane dissociation at higher temperatures promoted carbon-chain propagation toward higher hydrocarbon formation in the low-temperature hydrogenation, as depicted in Scheme 4 showing the proposed mechanism of methane homologation on Ru clusters in NaY.

Furthermore, it was demonstrated by EXAFS study that the average particle sizes of Ru in NaY (in terms of C.N. of Ru–Ru bond) remained unchanged before and after the methane deposition at 523–723 K and hydrogenation at 300–873 K. The zeolite microporous cages ef-
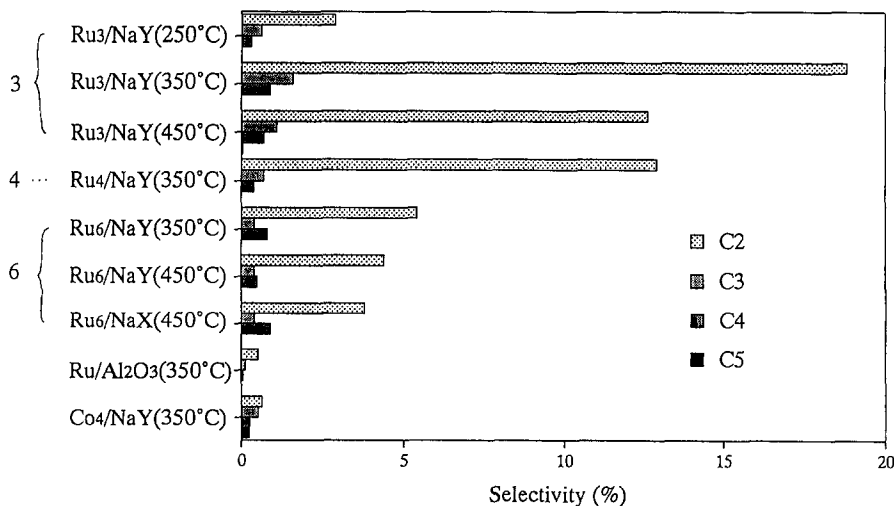

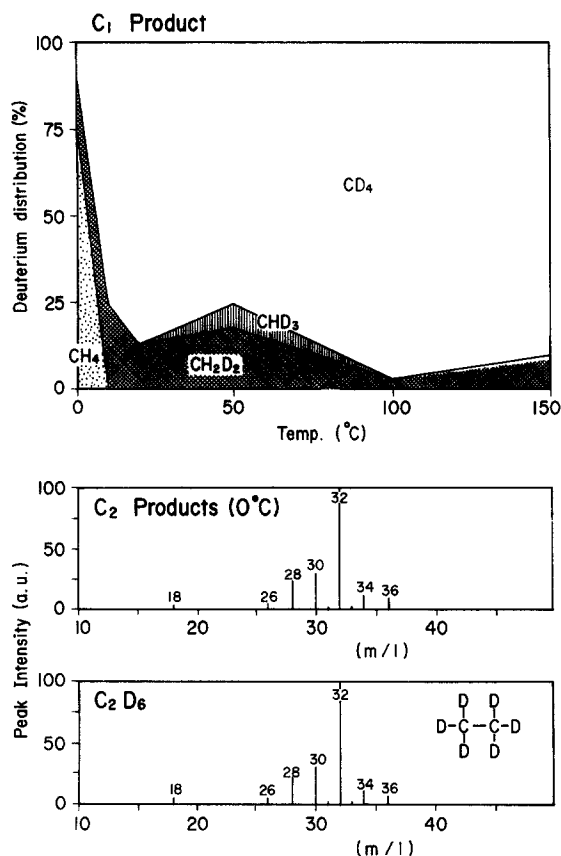Fig. 10. Selectivity of the various catalysts.

Fig. 11. The deuterium distribution of methane (C_1 product) and ethane (C_2 product) produced by ramping the temperature from 300–523 K in a D_2 flowing on Ru catalyst (C.N. = 6.7; 10 Å) derived from $Ru_3(CO)_{12}$/NaY evacuated after the methane deposition at 623 K. The deuterium distribution of C_1 and C_2 products were analyzed by GC/mass spectrometry.
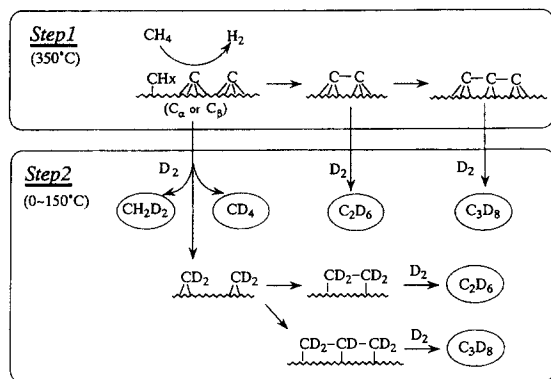
Scheme 4.

fectively resisted the sintering of Ru clusters which were accommodated by intrazeolitic constraint.

4. Conclusions

(1) The coordinately unsaturated Rh capping V_4O_{12} and V_6O_{19} cluster frameworks are catalytically active for the selective oxidation of propene towards acetone, possibly due to a bifunctional role consisting of Rh and vanadate cluster moieties as molecular modeling of supported metal catalysts.

(2) The CO-photoreduction of silica-impregnated [(RhCp*)$_4$ Mo$_4$O$_{16}$] (I) resulted in the formation of two sets of carbonyls attached to Rh (ν_{CO} = 2092 and 2035 cm^{-1}) and Mo sites (2061 and 2021 cm^{-1}). The EXAFS, FTIR and TPD results suggested that the 4c bridged Mo–O bonds were selectively reduced with CO. All the carbonyls were completely removed by the thermal evacuation at 434 K, leaving oxygen-deficient sites of Mo atoms which exhibit high activities for the propene metathesis reaction. The CO photoreduction of the incomplete cubane-type [(RhCp*)$_2$Mo$_3$O$_9$(OMe)$_4$] (II) produces the local active sites with higher catalytic activities for the reaction to make ethene and 2-butenes, rather than the compete cubane-type [(RhCp*)$_4$Mo$_4$O$_{16}$] (I) as a precursor.

(3) Ru$_3$(CO)$_{12}$, H$_4$Ru$_4$(CO)$_{12}$, [HRu$_6$(CO)$_{18}$]$^-$, Co$_4$(CO)$_{12}$, Rh$_6$(CO)$_{16}$, and [Pt$_3$(CO)$_3$(μ_2-CO)$_3$]$_n^{2-}$ (n = 3, 4) were synthesized by 'ship-in-bottle' technique in NaY zeolite micropores. Highly dispersed Ru, Co and Pt catalysts were prepared by removal of carbonyls by thermal evacuation at 323 K, followed by H$_2$ reduction. The carbon species [CH$_x$] (x = 0–3) are deposited on naked metal clusters in NaY by admission of methane at 423–623 K, which are completely converted by hydrogen at 300–423 K to C_1–C_5 hydrocarbons without any formation of graphitic carbons. The yields of C_2^+ hydrocarbons in methane homologation were affected as follows; Ru$_3$/NaY < Ru$_4$/NaY

$< \text{Ru}_6/\text{NaY} < \text{Ru (50 Å) on NaY}$; The reactivity of surface carbon bound to metal clusters and mechanism for C–C bond formation were discussed in conjunction with size effects of Ru clusters and chemical interaction in NaY micropores.

References

[1] M. Ichikawa, Adv. Catal., 38 (1992) 283–400.
[2] N. Herron, Y. Wang, G.D. Stucky, M.M. Eddy, D.E. Cox, T. Bein and K. Moller, J. Am. Chem. Soc., 111 (1989) 530.
[3] M. Ichikawa, in K. Tamaru (Ed.), Dynamic Aspects in Heterogeneous Catalysis, Plenum, New York, 1994, p. 149–214; CHEMTECH, (1982) 674; Polyhedron, 7 (1983) 235.
[4] M. Ichikawa, L.-F. Rao, T. Kimura and A. Fukuoka, J. Mol. Catal., 62 (1990) 15.
[5] M. Ichikawa, Polyhedron, 7 (1983) 235; A. Fukuoka, L.-F. Rao, N. Kosugi, H. Kuroda and M. Ichikawa, Appl. Catal., 50 (1989) 295.
[6] A. Fukuoka, T. Kimura, N. Kosugi, H. Kuroda, Y. Minai, Y. Sakai, T. Tominaga and M. Ichikawa, J. Catal., 126 (1990) 434.
[7] M. Ichikawa, F.-S. Xiao, C.G. Magpanty, A. Fukuoka, W. Henderson and D.F. Shriver, Stud. Surf. Sci. Catal., 61 (1991) 297; W.M.H. Sachtler and M. Ichikawa, J. Phys. Chem., 90 (1986) 475.
[8] F.-S. Xiao, A. Fukuoka and M. Ichikawa, J. Catal., 138 (1992) 206.
[9] M. Ichikawa, A.M. Liu, G. Shen, T. Shido, Top. Catal., 2 (1994) 141.
[10] K. Isobe and A. Yagasaki, Acc. Chem. Rev., 26 (1993) 526; Y. Hayashi, K. Toriumi and K. Isobe, J. Am. Chem. Soc., 110 (1988) 3666.
[11] Y. Do, X. You, C. Zhang, Y. Ozawa and K. Isobe, J. Am. Chem. Soc., 113 (1994) 5892; Y. Hayashi, Y. Ozawa and K. Isobe, Chem. Lett., (1989) 425.
[12] L.-F. Rao, A. Fukuoka, N. Kosugi, H. Kuroda and M. Ichikawa, J. Phys. Chem., 94 (1990) 5317.
[13] P. Gelin, Y.B. Taarit and C. Naccache, J. Catal., 59 (1979) 357.
[14] G. Begeret, P. Gallezot and F. Lefebre, Stud. Surf. Sci. Catal., 28 (1986) 401.
[15] S. Kawi and B.C. Gates, J. Chem. Soc., Chem. Commun., (1991) 994; P.-L. Zhou and B.C. Gates, J. Chem. Soc., Chem. Commun., (1989) 347.
[16] A.M. Liu, T. Shido and M. Ichikawa, J. Chem. Soc., Chem. Commun., (1995) 507.
[17] G.-J. Li, T. Fujimoto, A. Fukuoka and M. Ichikawa, Catal. Lett., 12 (1992) 171.
[18] R.-J. Wang, T. Fujimoto, T. Shido and M. Ichikawa, J. Chem. Soc., Chem. Commun., (1992) 962.
[19] M. Ichikawa, L.-F. Rao, N. Kosugi, T. Ito and A. Fukuoka, Faraday Discuss. Chem. Soc., 87 (1989) 232.
[20] T. Yamamoto, T. Shido, S. Inagaki, T. Fukushima and M. Ichikawa, in press.
[21] M.C. Coaraway and B.E. Hanson, Inorg. Chem., 25 (1986) 1445.
[22] H. Mimoum, J. Mol. Catal., 7 (1980) 1.
[23] H. Mimoum, M.M. Perez Machirant and I. Seree de Roch, J. Am. Chem. Soc., 100 (1978) 5437.
[24] J.W. McMillan, H.E. Fischer and J. Schwartz, J. Am. Chem. Soc., 113 (1991) 4014.
[25] R. Psaro, R. Ugo, B. Besson, A.K. Smith and J.M. Basset, J. Organomet. Chem., 213 (1981) 215.
[26] C.C. Williams and J.G. Ekerdt, J. Phys. Chem., 97 (1993) 6843.
[27] V.B. Kazansky, B.N. Shelimov, K.A. Vikulov, Proc. 10th Int. Congr. Catal., Hungary, 1992, p. 515.
[28] T. Koerts, M.J.G. Deelen and R.A. van Santen, J. Catal., 138 (1991) 101.